VIV of Tapered Cylinders: 3D LES Numerical Simulation

Khosrow Bargi [1], Vahid Tamimi[2*], Mostafa Zeinoddini[3]

[1]*professor, School of Civil Engineering, College of Engineering, University of Tehran, Tehran, Iran;* kbargi@ut.ac.ir
[2]**Ph.D Student, School of Civil Engineering, College of Engineering, University of Tehran, Tehran, Iran;* Vahid.Tamimi@ut.ac.ir
[3]*Associate professor, Department of Civil Engineering, K.N.Toosi University of Technology, Tehran, Iran;* Zeinoddini@kntu.ac.ir

ARTICLE INFO	ABSTRACT
	In the present study, the author's previous experimental investigations on the vortex induced vibration of uniform and tapered circular cylinders are numerically simulated. The circular cylinders have medium mass ratios (5.93, 6.1), low mass-damping parameters (0.0275, 0.0279) a mean diameter of 0.028m and an aspect ratio of about 14. A fully coupled two-way fluid-structure interaction (FSI) analysis is used to simulate the phenomena of vortex induced vibration in vicinity of the lock-in range. The 3D computational fluid dynamic (CFD) model is employed to solve the incompressible transient Navier-Stokes equations. LES-Smagorinsky turbulent model is considered within all simulations. Structural displacements are calculated through transient structural analysis in mechanical application (Computational Structural Dynamics-CSD). The transverse vibrations of uniform and tapered cylinders are compared against the experimental results. The comparison reveals that the model is capable to reasonably well predict the initial and upper branches of the responses. It, however, falls short to properly predict the lower branch. The simulation results of the fixed and elastically mounted tapered cylinders indicate that the flow field, in the case of the elastically mounted tapered cylinder, is completely different from that for the equivalent fixed tapered cylinder. For the case of the elastically mounted tapered cylinder no vortex cell fond to be forming in the lock-in region and a single frequency response dominated the entire length of the cylinder.

1. Introduction

Significant developments in the offshore oil industry have enabled us to move further offshore in search for oil or gas reservoirs. Offshore platforms progressed from the fixed structures installed in shallow waters to the gigantic floating platforms like semi-submersibles and FPSOs for production or tension-leg and spar platforms for drilling operations in the so called ultra-deep waters. Tapered circular cylinders or truncated cones are employed as the structural elements in these platforms and in a variety of other offshore engineering applications. Common examples are legs of the gravity based oil/gas platforms, main shafts of the offshore wind energy turbines, industrial chimneys, light houses and broadcasting towers. While being geometrically simple, this configuration creates a complex flow pattern in the near wake of the structure [1].

The challenge is the operation of a massive dynamic system under severe conditions of wind, sea currents and waves. One of the major problems during offshore operations is the vibration induced on the risers and platforms by sea currents. As water flows around the body it excites the structure into several modes of vibration that vary with the structural properties of the system. This is called Vortex induced Vibration or VIV. In the long term the structural integrity of the risers can also be compromised due to structural fatigue.

Vortex induced vibration (VIV) is a complex multi-physics problem which concerns with both structural and fluids fields. There are three main different approaches toward the VIV problems. i) experimental studies ii) semi empirical modelling iii) numerical simulations. Experimental investigation of VIV, when particularly looking for vortex patterns behind the

cylinders, is costly and time consuming. This is especially the case when using methods to provide both qualitative and quantitative data like Digital Particle Image Velocimetry or DPIV. Instead, if correctly simulated, the numerical methods will make vortex pattern studies at the wake of the cylinders much easier.

Numerical simulation of flow field at the wake of fixed or forced vibrating cylinders are relatively straightforward compared to resonance vortex induced vibration simulation of an elastically mounted cylinder from rest. The difficulty lies in accurate simulation of the fluid field and correct coupling of two structural and fluid fields to let the vortices become synchronizes with the cylinder oscillation across the lock-on range. This is why most previous numerical researches were concentrated on vortex shedding studies and force measurements on fixed or forced vibrating cylinders [2].

The self excited transverse vibration amplitudes of two dimensional (2D) numerical simulations in the Blackburn and Karniadakis [3] and Newman and Karniadakis [4] works with low mass-damping or even zero damping parameters, at low Reynolds numbers of Re=100 to 200, were smaller than the expected values. They both used a spectral method in which the computational mesh was fixed to the cylinder. Zhang and Dalton [5] conducted a 2D LES (Large Eddy Simulation) investigation of one degree of freedom (transverse) cylinders at Re=13,000. The maximum reduced amplitude of about 0.26 was reported for their system with a damping ratio of 0.02. Saltara et al. [6] numerically simulated VIV (self excited) of a flexible cylinder at Re=1,000. They used a combined discrete-vortex/LES method to describe the flow field. The maximum transverse amplitude was equal to A/D=0.7. Evangelinos et al. [7] conducted a three dimensional (3D) direct numerical simulation (DNS) study on flexible cylinders with one degree of freedom at Re=1,000. Tutar and Holdo [8] conducted a 3D finite-element LES on the forced oscillation of cylinders at Re=24,000. They reported that the 3D representation of vibrating cylinder was necessary to get more accurate results. They also found that the 3D simulation of the forced oscillation of a cylinder would provide better agreement with experimental data compared to 2D calculations.

Guilmineau and Queutey [9] simulated VIV (self excited) of an elastically mounted rigid cylinder with low mass-damping. The mass ratio was 2.4, the mass-damping was 0.013 and Re ranged from 900 to15,000. They solved the incompressible 2D K-ω Reynolds-Averaged Navier–Stokes (RANS) equations to simulate the flow field. Al-Jamal and Dalton [10] presented the results of a 2D LES simulation of VIV of a circular cylinder in uniform flow (Re=8,000). Their investigation was focused on two different mass ratios (1.68, 7.85) and different damping ratios (0-

0.1). The cylinder response at mass-damping of 0.157 was reported to follow the typical VIV response of low mass ratio cylinders. Much recently Saltara et al. [11] conducted 3D CFD simulation of VIV of a free transverse oscillating cylinder. They used detached eddy simulation (DES) turbulence model for Reynolds number of around 10,000. They reported good agreement between the numerical results and experimental data for their small mass damping (0.00858) system.

As it may be noticed, studies reported above were dealing with the vortex shedding past or VIV of uniform cylinders. Literature on experimental and numerical modeling of the flow and vortex shedding past tapered, as compared to straight uniform circular cylinders, is very scarce. This is probably because of complexity and three dimensionality of the wake behind a tapered cylinder, which are difficult to be properly quantified and captured in experiments and simulations. With a tapered cylinder the local Reynolds and Strouhal numbers, even under a uniform flow, vary in the span-wise direction. A range of flow-regimes such as steady, laminar unsteady and turbulent wakes may coexist in the same geometry. At higher Reynolds numbers the physics in the near wake become even more complex.

Vortex shedding around tapered cylinders in laminar flows was numerically simulated by Jespersen and Levit [12]. Valles et al. [13] numerically simulated vortex shedding in tapered circular cylinder with laminar flow at low Reynolds numbers of 130 to 180 (based on larger diameter of the cylinder). The simulation results showed very good agreement with experimental data. Parnaudeau et al. [14] also carried out IBM (immersed boundary method) direct numerical simulations of vortex shedding in tapered cylinders. Narsimhamurthy et al. [15] simulated a tapered cylinder using the IBM. They addressed some vortex characteristics behind tapered cylinders such as vortex dislocation. Their predictions for the Strouhal number versus the local Reynolds number, however, did not accurately follow the experimental results.

Tamimi et al. [16] conducted a 3D simulation of vortex shedding past fixed tapered circular cylinders at subcritical Reynolds numbers. The computational mesh of the numerical model was calibrated with others DNS and experimental results. Certain proportions between the length and diameter of the cylinder and the optimum number of span-wise and planar mesh divisions were introduced. Reasonable quantitative agreements were obtained between the model predictions and the experimental results from other researchers.

Most previous experimental studies and almost all previous numerical simulations on tapered circular cylinders were concentrated on the flow field in the wake of the fixed cylinder and vortex shedding patterns [1].The results provide useful information on

main flow characteristics for tapered cylinders such as vortex dislocations and splitting, cellular vortex shedding and oblique vortex shedding [13], [17].

Two most distinct experimental studies on tapered cylinders are the works carried out by Hover et al. [18] and Techet et al. [19]. Hover et al. [18] measured forces at both ends of rigid cylinders experiencing cross-flow oscillations in water stream at Reynolds number of 3,800. Forced harmonic motions and free vibrations of uniform and tapered cylinders were recorded. Free vibration experiments on a tapered cylinder (with mass ratio of 4 and taper ratio of 40) showed that the regime of low correlation was elongating to higher reduced velocities. Techet et al. [19] experimentally studied the flow in the wake of forced vibrating tapered circular cylinders in the MIT towing tank. The Reynolds numbers ranged from 400 to 1500. They reported that no vortex cell was forming in the lock-in region and that a single frequency response dominated the entire spanwise length. They also found that within certain parametric ranges there was a combination of 2S mode vortices around the larger diameter and 2P mode vortices around the smaller diameter ends.

In the present study, self excited transverse response of elastically mounted uniform and tapered circular cylinders are numerically simulated. The cylinders have a medium mass ratio (5.93, 6.1) and low mass-damping parameters (0.0275, 0.0279). The Reynolds number, based on mean diameter of the cylinders, ranges from 4,200 to 11,200.The model replicates an in-water towing tank experimental study conducted by the authors to investigate the VIV response of tapered cylinders. Numerical results for the transverse vibrations of uniform and tapered cylinders are compared against the experimental data. The main focus of the present study is on the transverse responses magnitude, flow field characteristics and the vortex patterns at the wake of elastically mounted tapered circular cylinders.

2. Model Basis

In this section the basic elements of the 3D numerical model characteristics are described. There are two main strategies for the analysis of fluid-structure interaction phenomena with in-stationary flows described by the Navier-Stokes equations: i) partitioned solution ii) simultaneous solution strategy. In the partitioned solution different solvers for fluid and structure are called sequentially. Loosely coupled (explicit) solutions are followed if the solvers are called once per time step [20, 21]. In strongly coupled (implicit) solutions an additional FSI-iteration loop is introduced in which the solution of fluid and structure is repeated until the convergence of interaction forces and displacements [22, 23]. In contrast, simultaneous solution procedures [24-26], which are also called as matrix coupled or monolithic formulations, consider

the coupled system as a whole and solve it in a single software environment. The entire set of governing equations is formulated and solved in a single matrix equation system applying a single equation solver and iteration loop.

Hubner and Seidel [27] declared that loosely coupled partitioned solution procedures are very efficient if the coupling is weak or if time scales of fluid and structure differ strongly. In contrast, for large structural displacements or if a considerable fluid mass is moving with the structure, at least strongly coupled partitioned solution procedures (with FSI iteration loop) have to be applied [27].
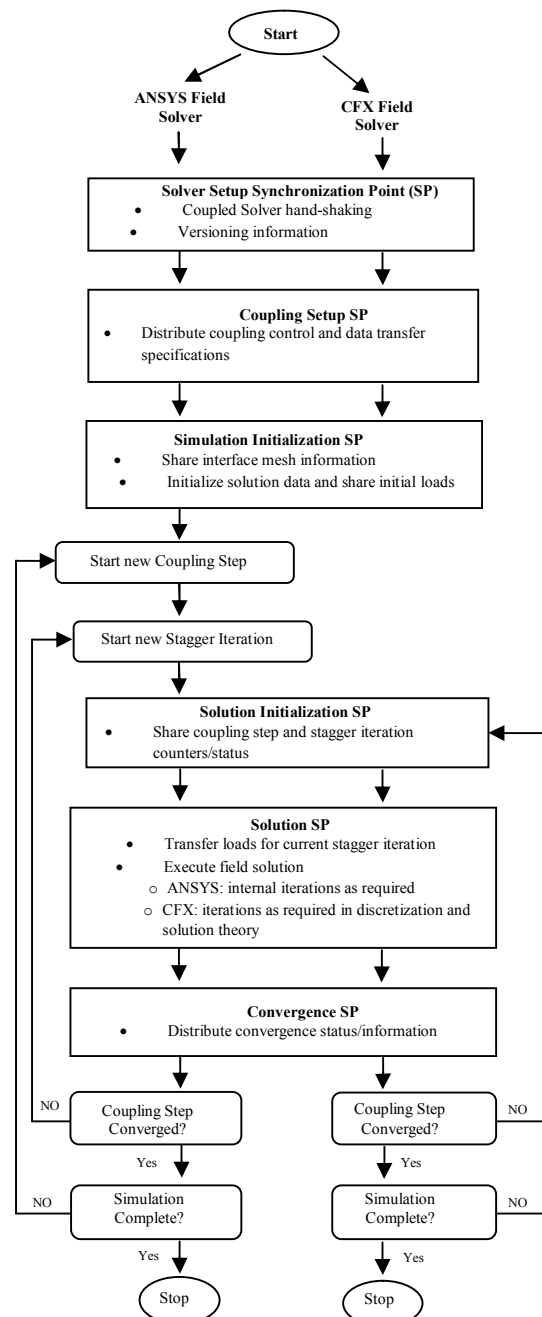

Figure 1. Sequence of synchronization points [28]

Hubner and Seidel [27] stated that simultaneous solution procedures are preferable in order to ensure efficiency, stability and convergence of the coupled

solution. But in the present time, a commercial analysis software based on a monolithic approach to FSI which allows for simultaneous solutions of non-linear structures and complex three-dimensional flows, is not available. Therefore, in this paper a fully coupled two-way FSI analysis is used to simulate the VIV phenomena in the vicinity of the lock-in range. The Fluid-Structure Interaction (FSI) is solved with ANSYS-CFX12. The computational fluid dynamics (CFD) model is used to solve the 3D incompressible transient Navier-Stokes equations of the fluid domain [28]. Structural displacements are calculated through transient structural analysis for mechanical applications (computational structural dynamics-CSD). The transient structural analysis solver is the Mechanical application module of ANSYS. Interactions between CSD and CFD analyses are considered at the fluid-structure interfaces. Forces at the fluid-structure interface, computed from CFD solution, are passed to the structural model as loads. Structural displacements from CSD solution are transferred to the fluid boundary part of the fluid-structure interface to change the fluid domain mesh. In two-way FSI, communicating data between CFX and the Mechanical application modules is automated by the MFX branch of the ANSYS Multi-field solver. In this branch of the ANSYS Multi-field solver, data is communicated between the CFX and the Mechanical application field solvers through standard internet sockets using a custom client-server communication protocol. This custom solution maximizes execution efficiency and robustness, and greatly facilitates future extensibility. Coupled simulations begin with the execution of the Mechanical application and CFX field solvers. The Mechanical application solver acts as a coupling master process to which the CFX-Solver connects. Once that connection is established, the solvers advance through a sequence of six pre-defined synchronization points (SPs), as illustrated in Figure 1. At each of these SPs, each field solver gathers the data it requires from the other solver in order to advance to the next point. The first three SPs are used to prepare the solvers for the calculation of intensive solution process, which takes place during the final three SPs. These final SPs define a sequence of coupling steps, each of which consists of one or more stagger/coupling iterations. During every stagger iteration, each field solver gathers the data it requires from the other solver, and solves its field equations for the current coupling step [28]. At each time step the stager iteration is continued until the coupling step is converged. During each stager iteration, each of fields' solvers (CFD or CSD) gathers the data they need from other solver and solve their equation for the current

coupling step. Stagger iterations are repeated until the data transferred between solvers and all field equations converge or a maximum number of stagger iterations is reached (that is about 100 iterations). This will make the VIV simulation a very time consuming task (as compared to vortex shedding simulations). So it is reasonable to incorporate any desirable changes in the flow field (like changes to the inlet velocity) in the CFD solver and then introduce the changed flow field to the FSI simulation as an initial condition.

The computational mesh consists of two blocks. The first block encircles the cylinder and consists of fine regulated hexahedron elements. The unstructured second block surrounds the first block and consists of mostly hexahedrons and a few prism elements. A grid sensitivity study has first been performed. In order to avoid repetition the reference is made to the authors' previous study [16, 29]. Tamimi et al. [16] considered different computational mesh resolutions, varying in both planar and the spanwise directions of the domain. It was shown that the number of spanwise divisions has a remarkable effect on the models' predictions. In the selection of the most optimum grid refinement the computational cost was also considered. The results of the analysis show that the computational grid described in Table 1 provides reasonable agreement with the experimental results of some other researchers (Tamimi et al. [16]). The discretization characteristics of the computational domain, including the thickness of the first inflation layer and number of span-wise divisions are summarized in Table 1. The table also gives the total number of nodes, the total number of elements and the wall clock time for computing 600 time steps on an Intel (R) Core™ i7 CPU 950 @ 3.07GHz personal computer (with 6 GB of RAM). As it might be noticed in Table 1, considerable amount of time was necessary to perform a single analysis.

It is noted that the 600 time steps specified in Table 1 is just a measure value. The exact values of time steps used to compute the averaged flow in each of the flow velocities are around 2000. Table 1 also indicates that the efficiency of the parallel run relative to a serial run, assuming that the problem is stationary, is around 35%, which does not seem very high. This is partly because the performance determination is not sometimes straightforward due to the fact that only part of the solver run is actually performed in parallel. The reading and distributing of the solver input file data, and the collecting and writing of results file data are highly I/O dependent and not parallelized. These stages, therefore, depend on high disk speeds and fast network communication for fast operation. Time stepping and convergence also play a role in the computation performance [30].

Table 1. Details of the computational mesh resolutions.

Mean diameter of the cylinder	Thickness of the first inflation layer (m)	Number of span-wise divisions	Number of elements	Number of nodes	y^+	Wall clock time for 600 time steps (hours)	
						Parallel Runs (8 partitions)	Serial Runs
D_{mean}	0.001 D_{mean}	140	1,465,940	1,498,548	1.5	176	274

The 3D computational domain used for VIV simulation of the tapered cylinder is depicted in Figure 2. The domain dimensions are also provided in the figure. To avoid the end effects, identical heights are considered for the cylinder and the computational domain (Figure 2).
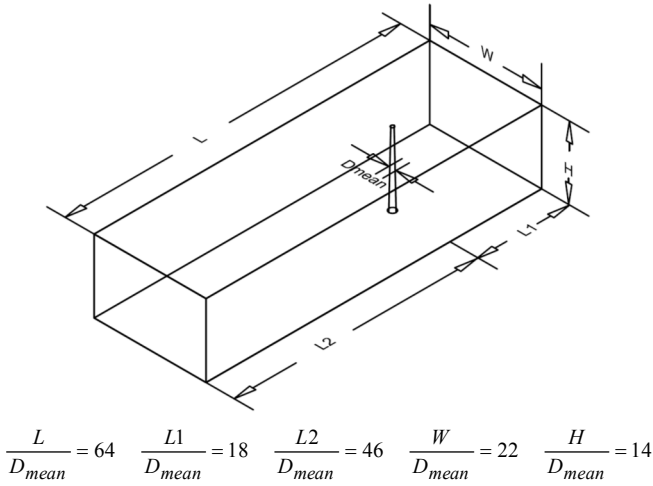

$$\frac{L}{D_{mean}} = 64 \quad \frac{L1}{D_{mean}} = 18 \quad \frac{L2}{D_{mean}} = 46 \quad \frac{W}{D_{mean}} = 22 \quad \frac{H}{D_{mean}} = 14$$

Figure 2. Overall view the computational domain.

A uniform velocity profile is imposed on the inlet boundary. A zero static pressure condition is used on the outlet boundary. In order to avoid flow disturbance at the boundaries, a free slip wall condition is prescribed for the upper and lower cylinder ends and on the longitudinal exterior wall boundaries. The time step used in these simulations is chosen between 1 and 3 percent of the vortex shedding period (in a fixed cylinder). All simulation results presented are based on the Large Eddy Simulation (LES) [31] turbulence model with Smagorinsky subgrid scale model [32]. Tamimi et al. [16] indicated that the LES-Smogorinsky model is able to provide predictions reasonably close to the experimental measurements. This appears in line with findings from other researchers. For example, Murakami [33] and Rodi [34] compared the capability of the LES model with other well known models like K-ε and Algebraic Stress models when simulating the flow around bluff bodies. They concluded that the LES model provides reliable and accurate simulations of the flow characteristics. With the Large-Eddy Simulation technique, a distinction is made between the large and small scale motions. The governing equations are then derived by filtering the time dependent Navier-Stocks equations in the physical domain. In this process, those eddies whose scales are smaller than the computational mesh dimensions are filtered out. Therefore, the final equations are dominated by the dynamics of the larger eddies. The filtered variable is defined by [28]:

$$\overline{\phi}(x) = \int_D \phi(x') \; G(x;x') \; dx' \tag{1}$$

Where D is the fluid domain, G is the filter function and $\overline{\phi}$ is the filtered variable. The unresolved part of a quantity ϕ is defined by:

$$\phi' = \phi - \overline{\phi} \tag{2}$$

The discretization of physical domain into finite control volumes will provide the filtering operation:

$$\overline{\phi}(x) = \frac{1}{V} \int_V \phi(x') \; dx' \qquad , x' \in V \tag{3}$$

Where V is the control volume. The filter function in the Eq. (3) is then [28]:

$$G(x, x') = \begin{cases} \dfrac{1}{V}, & x' \in V \\ 0 & otherwise \end{cases} \tag{4}$$

Eqs. (2) to (4) highlight the importance of the computational mesh resolution used in LES simulations, since the mesh size implicitly acts as a filtering mechanism for the small scale eddies.

By filtering the Navier-Stocks equations, the filtered incompressible momentum equation will be [28]:

$$\frac{\partial \overline{U}_i}{\partial t} + \frac{\partial}{\partial x_j}(\overline{U}_i \overline{U}_j) = -\frac{1}{\rho}\frac{\partial \overline{P}}{\partial x_i} + \frac{\partial}{\partial x_j}\left[\nu\left(\frac{\partial \overline{U}_i}{\partial x_j} + \frac{\partial \overline{U}_j}{\partial x_i}\right)\right] - \frac{\partial \tau_{ij}}{\partial x_j} \tag{5}$$

Where $\overline{U}$ is the fluid velocity, P is the static pressure, ρ is the fluid density and τ_{ij} is the subgrid-scale stress. The last parameter incorporates the small scales effect and is defined by [28]:

$$\tau_{ij} = \overline{U_i U_j} - \overline{U}_i \overline{U}_j \tag{6}$$

The large scale turbulent flow can be solved directly and the effects of the small scales are taken into account by choosing a suitable subgrid-scale model. In ANSYS CFX [28] an eddy viscosity approach is used which relates the subgrid-scale stresses τ_{ij} to the large-scale strain rate tensor $\overline{S}_{ij}$ in the following way:

$$-(\tau_{ij} - \frac{\delta_{ij}}{3}\tau_{kk}) = 2\nu_{sgs} \; \overline{S}_{ij} \quad ,$$
$$\overline{S}_{ij} = \frac{1}{2}(\frac{\partial \overline{U}_i}{\partial x_j} - \frac{\partial \overline{U}_j}{\partial x_i}) \tag{7}$$

Unlike in RANS modelling, where the eddy viscosity ν_{sgs} represents all turbulent scales, the subgrid-scale viscosity only represents the small scales.

Three models are available to provide the subgrid-scale (SGS) viscosity ν_{sgs}. They include i) Wall-Adapted Local Eddy-Viscosity model or WALE model (Nicoud and Ducros [35]), ii) Smagorinsky model (Smagorinsky [32]) and iii) Dynamic Smagorinsky-Lilly model (Germano et al. [36], Lilly [37]). The wall-adapted local eddy-viscosity model by Nicoud and Ducros [35] (LES WALE model) is an algebraic model like the Smagorinsky model. The WALE model produces almost no eddy-viscosity in wall-bounded laminar flows and is therefore capable to reproduce the laminar to turbulent transition. The Smagorinsky model is known for its high stability due to its damping effect. However, it does not take any feedback from the flow field for adjusting and tuning the model constants. The Dynamic Smagorinsky-Lilly model is based on the Germano-identity and uses information contained in the resolved turbulent velocity field to evaluate the model coefficient. However this method needs explicit (secondary) filtering and is therefore more time consuming than an algebraic model.

Effects of these LES subgrid-scale models on the simulation results were investigated in author's previous study [29]. It was shown that Smagorinsky model provides better predictions as compared to the Direct Numerical Simulation (DNS) results by Dong and Karniadakis [38] and experimental data.

The Smagorinsky model is an algebraic model for the SGS viscosity (ν_{sgs}). Based on dimensional analysis, the SGS viscosity can be expressed as:

$$\nu_{sgs} \propto l \; q_{sgs} \tag{8}$$

Where l is the length scale of the unresolved motion (usually the grid size $\Delta = (Vol)^{1/3}$) and q_{sgs} is the velocity of the unresolved motion. Based on an analogy to the Prandtl mixing length model, the velocity scale is related to the gradients of the filtered velocity:

$$q_{sgs} = \Delta |\bar{S}| \qquad Where \qquad |\bar{S}| = (2\bar{S}_{ij}\bar{S}_{ji})^{1/2} \tag{9}$$

This yields the Smagorinsky model [32] for the subgrid-scale (SGS) viscosity:

$$\nu_{sgs} = (C_S \Delta)^2 |\bar{S}| \tag{10}$$

With C_S the Smagorinsky constant. The value of the Smagorinsky constant for isotropic turbulence with inertial range spectrum of $E(k) = C_k \; \varepsilon^{2/3} \; k^{-5/3}$ is:

$$C_k = \frac{1}{\pi}(\frac{2}{3C_k})^{3/4} = 0.18 \tag{11}$$

For practical calculations, the value of C_S is changed depending on the type of flows and mesh resolution. Its value is found to vary between a value of 0.065 (channel flows) and 0.25. Often a value of 0.1 is used and has been found to yield the best results for a wide range of flows [28]. This is also the value used in current simulations.

Turbulent wall functions are required to treat the transition to laminar like flow close to solid walls. ANSYS CFX [28] offers three different wall treatment functions, based on different distance definitions, dimensionless wall distances, wall roughness and velocity scales. They include i) Standard wall function, ii) Scalable wall function and iii) Automatic wall function. The scalable wall function method adjusts the near wall treatment with mesh spacing in the near wall region. The automatic wall treatment method which lacks the drawbacks of the standard wall function can be run on arbitrary fine meshes and is appropriate for hydraulically smooth surfaces [28]. An automatic wall treatment function is used in all simulations reported in the current study.

Structural part of the simulation consists of either a uniform or a tapered circular cylinder. The aluminum tapered and uniform circular cylinders characteristics are given in Table 2. They replicate dimensions of cylinders used in previous experimental study carried out by authors (Zeinoddini et al. [1]). The experimental setup is schematically shown in Figure 3 (b). In the experiments, as it can be seen, an elastic support allows for a one degree of freedom oscillation of the cylinder in the cross flow direction. The elastic support consists of two parallel horizontal aluminium slabs (1 cm thick), which connect firmly to the carriage and cylinder, respectively. Two other parallel vertical spring steel blades are clamped at the ends to the horizontal slabs. This system enables the cylinder to vibrate just in one direction (Figure 3 (b)).

Table 2. Overall dimensions of the uniform and tapered cylinders (in both of the experiments and simulations).

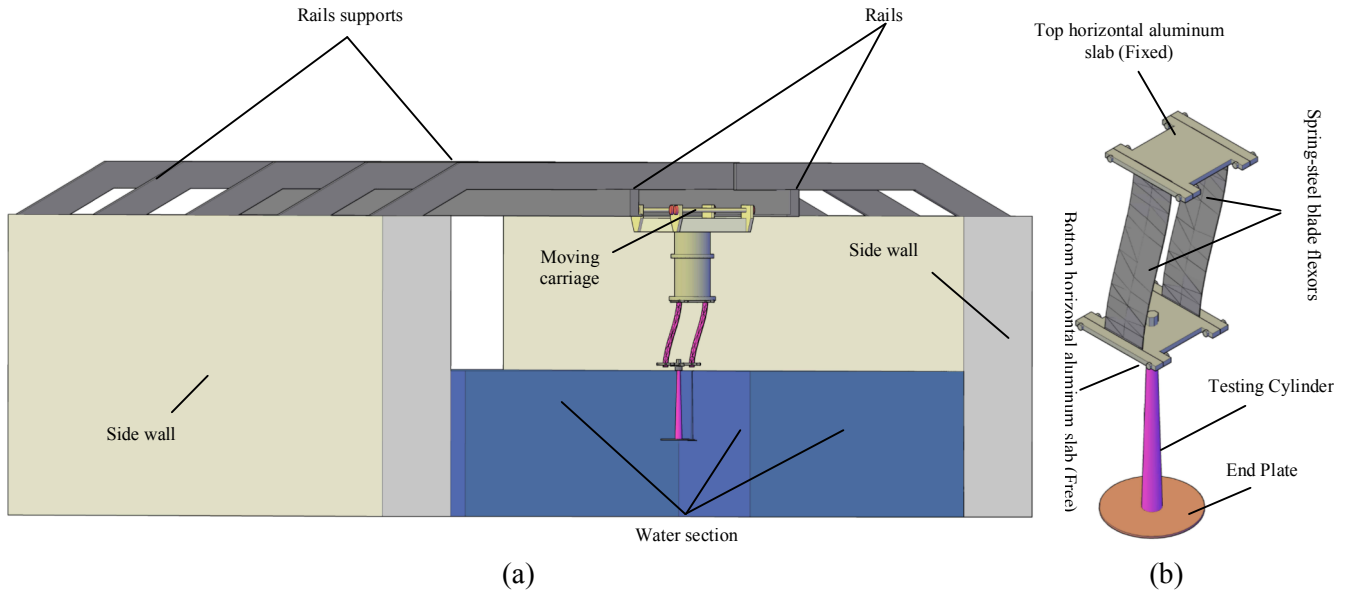| Cylinders | Cylinder properties | | | | | |
	Mid-span diameter, D_{mean} (mm)	Length, H (mm)	Taper ratio	Weight (gr)	Aspect ratio (H/D_{mean})	Material
Solid tapered cylinder	28	400	20	730	14.3	Aluminum
Solid uniform cylinder	28	400	-	670	14.3	Aluminum

(a)   (b)

Figure 3. (a). Schematic view of the experimental setup consist of an elastically mounted cylinder mounted to carriage, (the whole system is towed on two parallel rails on the top of the water tank); (b). Elastically mounted tapered cylinder with end plate.

Table 3. Oscillation characteristics of the tapered and uniform cylinders from the experiment.

Cylinders	m^*	f_N (in water)	ξ (in air)	$m^* \times \xi$
Uniform cylinder	5.93	1.2	0.00463	0.0275
Tapered cylinder	6.1	1.14	0.00456	0.0279

Table 4. The uniform and tapered models natural frequencies and damping ratios in water.

Cylinders	f_N (in water)		ξ (in water)	
	Experiment	Numerical model	Experiment	Numerical model
Uniform cylinder	1.2	1.44	3.3%	4.9%
Tapered cylinder	1.14	1.38	3.4%	2.5%

The overall structural characteristics of the vibrating system are given in Table 3. It should be noted that in calculation of the mass parameter, the mass of the plexiglas end plate (with diameter of 20 cm), vibrating horizontal solid slab on the top of the cylinder, bolts and vibrating portions of the spring blades are included.

In the simulation of the one degree of freedom oscillating cylinder, for simplicity reasons, the bending spring blades (in the experiments) are modelled with classical springs. Similar to that in the experiment, the linear structural stiffness of the springs in the numerical model remains equal to 210 N/m. Extra vibrating mass of end plates and oscillating parts of the elastic system, is included in the simulations as a lumped mass (1.94 kg).

To obtain the in-water natural frequencies of the vibrations of the cylinders, two numerical decay tests in water are conducted. Time histories of the in-water transverse vibrations of the tapered cylinder from a numerical decay test and the corresponding experimental decay test are shown in Figure 4. In-water natural frequencies and damping ratios of the uniform and tapered models are presented in Table 4. It is worth noting that in the case of experimental decay test, there is an end plate attached to the end of the cylinder. The end plate is not explicitly modelled in the numerical decay test. This might be a reason for

the slight difference between the numerical and experimental natural frequencies and damping ratios.
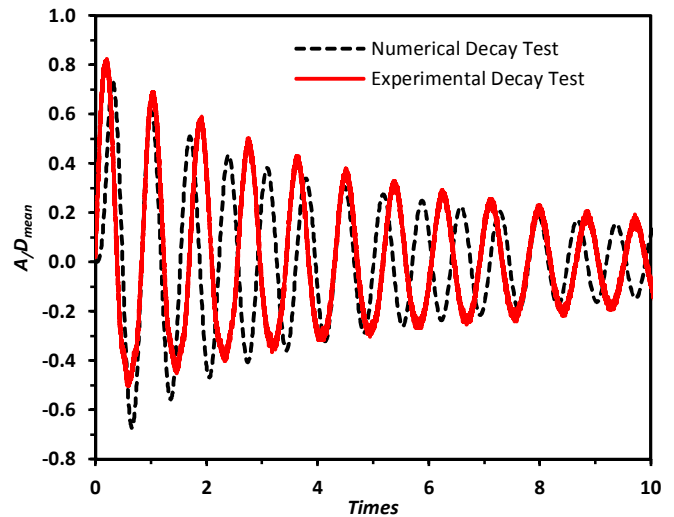

Figure 4. Comparison of the numerical and experimental decay test in-water for the tapered cylinder.

3. Numerical Results

In the following sections the results obtained from numerical simulation of the previously discussed VIV experiment will be presented. In section 3.1 the transverse vibrations of uniform and tapered cylinders are compared with available experimental data. The Reynolds number, based on mean diameter of the

cylinders, ranges from 4,200 to 11,200. Time histories of transverse vibrations of the elastically mounted uniform and tapered cylinders are also provided. Lift and drag force coefficients of the elastically mounted tapered cylinder is included in section 3.1. In sections 3.2-3.5 the flow field at the wake of an elastically mounted and a fixed tapered cylinder in lock-in range are presented and compared.

3.1. Simulating the experiment

The numerical and experimental reduced amplitudes of transverse vibration of uniform and tapered cylinders are presented in Figure 5-a. Figure 5-b provides the same for the frequency ratios. The cylinders structural characteristics are given in Table 2 and 3. Figure 5-a indicates that the numerical simulations of initial and upper branch of the transverse vibration seem to be acceptable as they are in a reasonable agreement with the experimental data. In general the numerical model underestimates the peak amplitude for the transverse vibration In the order of around 30%. This might be attributed to the fact that the vortex synchronization along the cylinder

and the lock-in phenomena was fully developed in the experiment. The time duration of the numerical modelling due to economical reasons, is considerably shorter than that in the experiment so the previously mentioned phenomena might not have been fully developed and might have been resulted in under predicting the peak responses. As shown in Figure 5-a, the predicted numerical lock-in range for the uniform cylinder is comparable with the experimental range ($4 < V_r < 10$). Figure 5-a shows that for both of the uniform and tapered circular cylinders the numerical simulations fall short to accurately predict the lower branch of the response. A similar shortcoming was also reported by other researchers who tried to numerically simulate the cylinder vibrations from the rest with constant flow velocity (Blackburn and Karniadakis [3], Newman and Karniadakis [4], Saltara et al. [6] and Guilmineau and Queutey [9]). Figure 5-b, however shows that, with both the uniform and tapered cylinders, the numerical predictions for the frequency ratios are in a good agreement with their corresponding experiments.
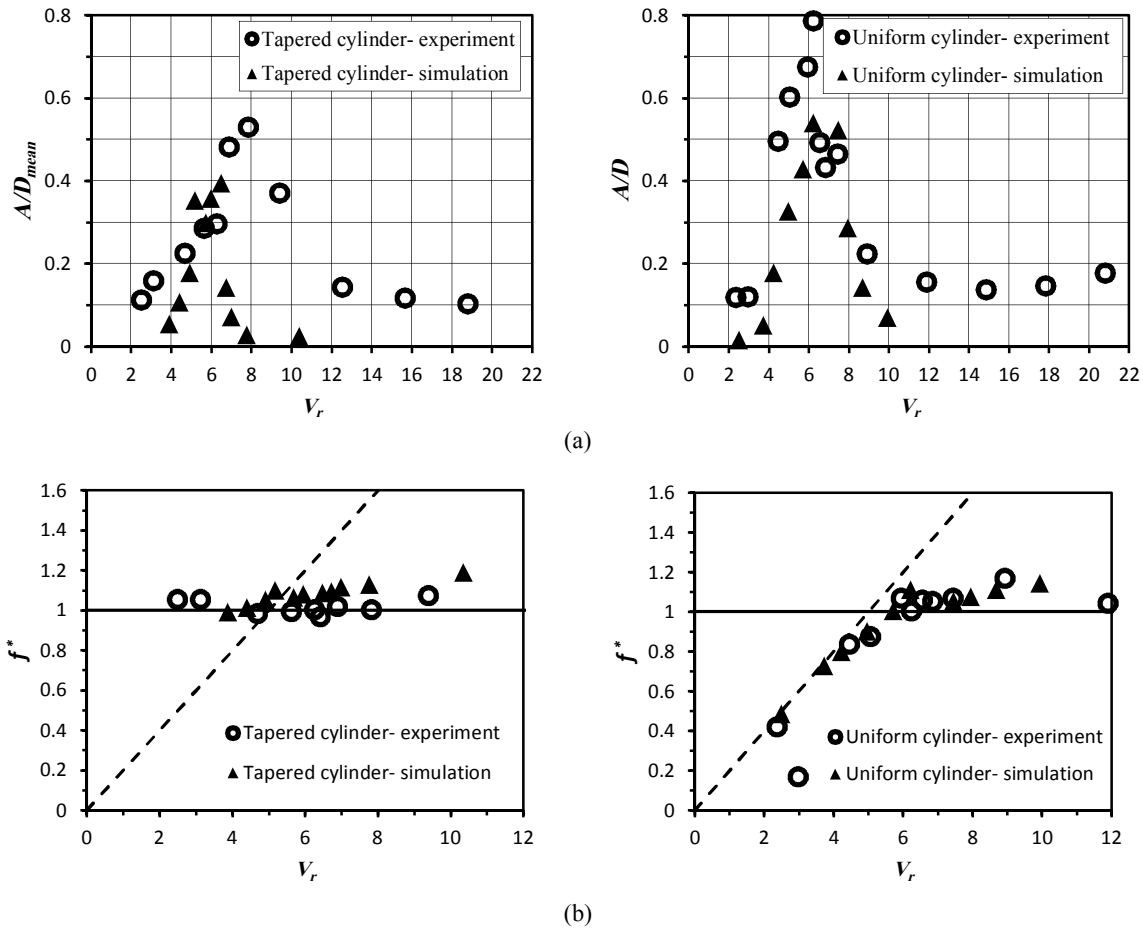

(a)

(b)

Figure 5. Numerical and experimental results for (a) transverse reduced amplitude and (b) frequency ratio of uniform (right) and tapered (left) cylinders.

Typical time histories of transverse vibrations of the tapered cylinder from the simulations and from the experiments are shown in Figure 6. They belong to tests with different flow velocities of 0.15, 0.2, 0.25 and 0.3m/s. Figure 7 provides the same for the uniform test cylinder. Typical frequency contents of experimental and numerical transverse vibrations of the tapered cylinder are shown in Figure 8. The Power Spectral Densities (PSDs) are produced by Fast Fourier Transform (FFT) of the responses and correspond to two sample reduced velocities of 5.17 and 6.47. As it may be noticed, the dominant frequency of both the experimental and numerical transverse vibrations of the tapered cylinder is close to each other. As it can be seen the experimental response demonstrates some small peaks at higher frequencies. The frequency of the second peak is around 2 time of that for the first peak. This might indicate on the presence of some small degrees of in-line vibrations in the experiments. The numerical model however lacks these types of fluctuations. The numerical results for the lift and drag force coefficients of the elastically mounted rigid tapered cylinder are also provided in Table 5.
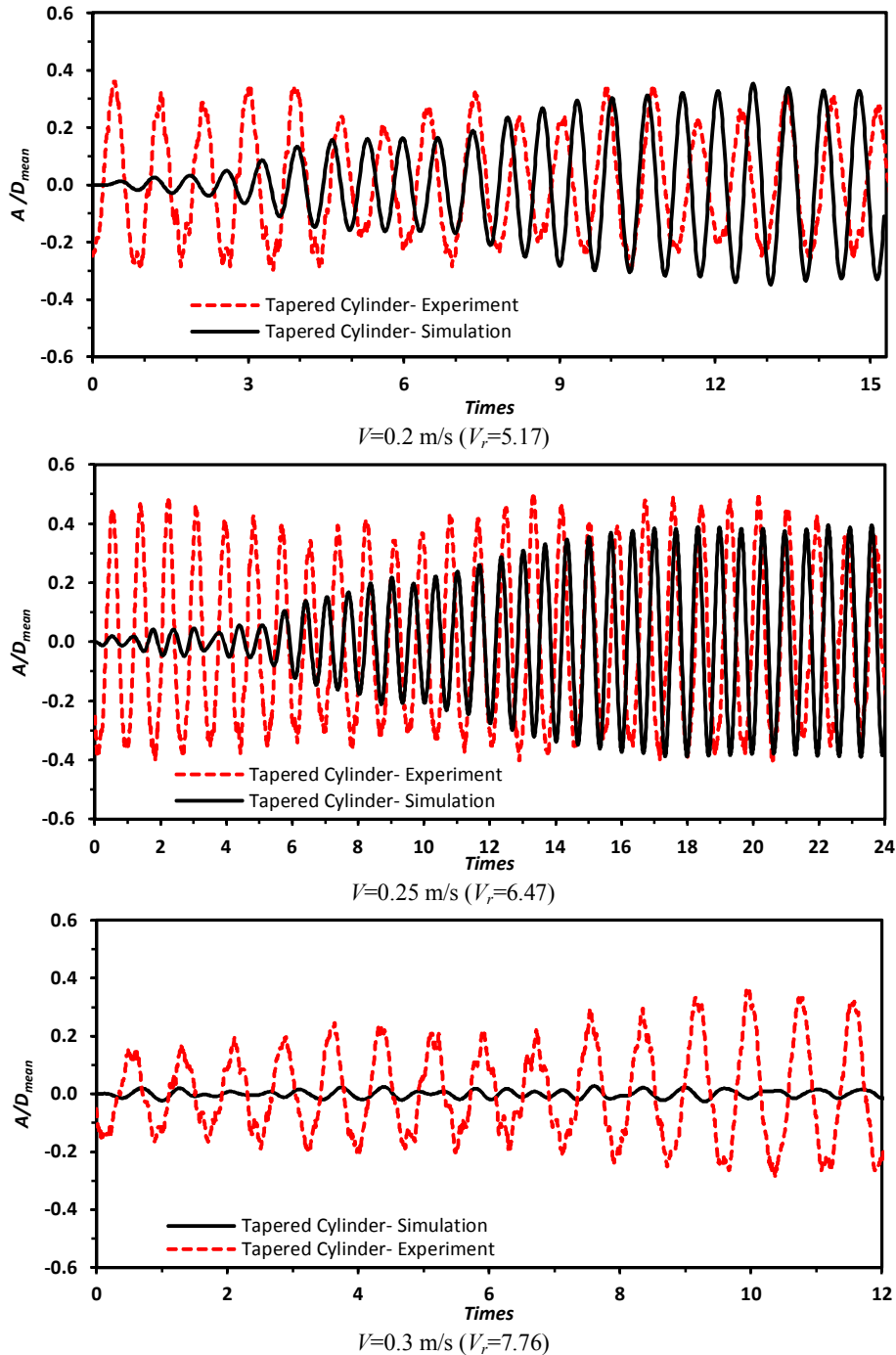

V=0.2 m/s (V_r=5.17)

V=0.25 m/s (V_r=6.47)

V=0.3 m/s (V_r=7.76)

Figure 6. Comparison of experimental and numerical time series of the transverse vibration of the tapered cylinder.
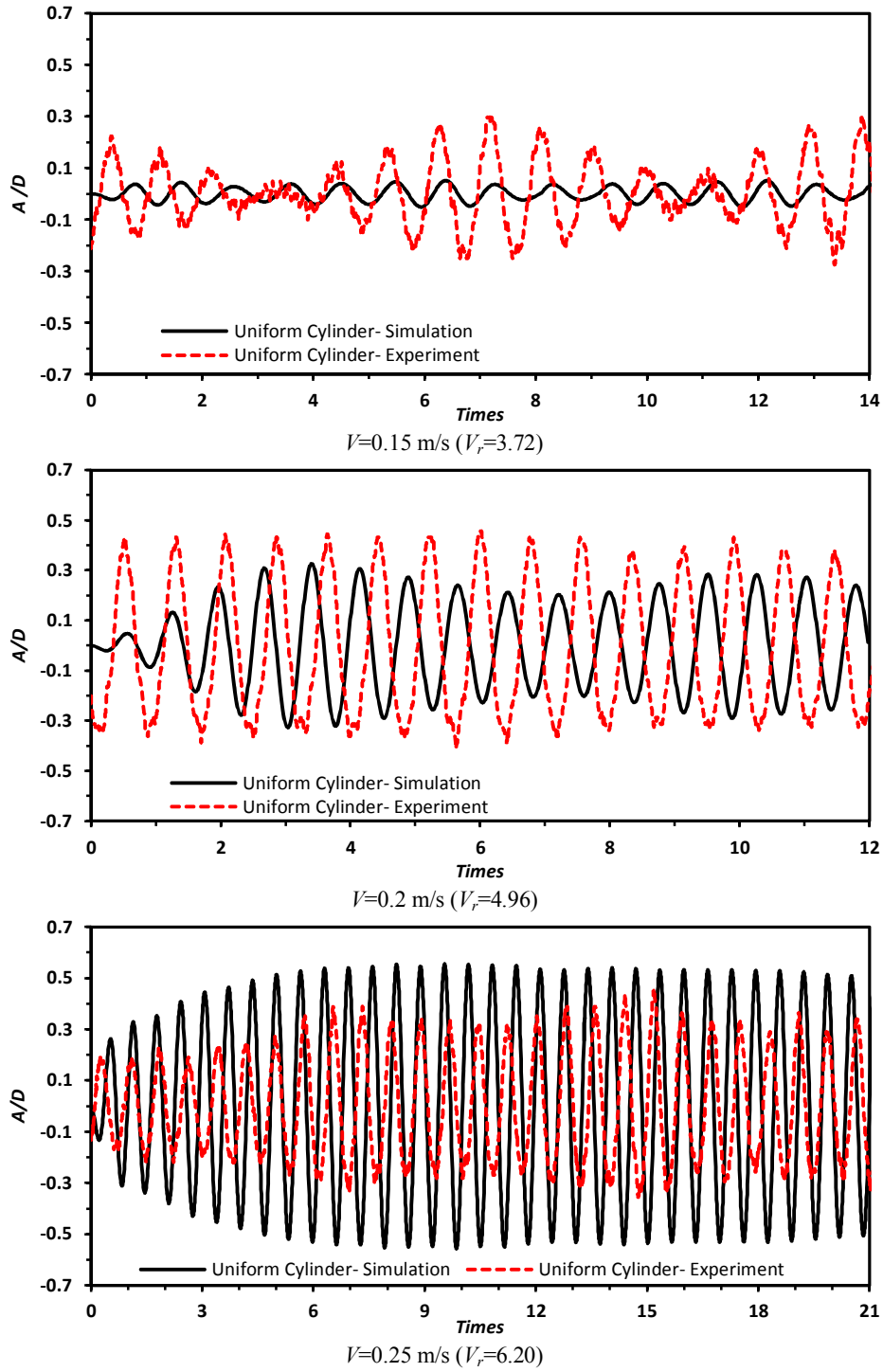
V=0.15 m/s (*V*$_r$=3.72)

V=0.2 m/s (*V*$_r$=4.96)

V=0.25 m/s (*V*$_r$=6.20)

Figure 7. Comparison of experimental and numerical time series of the transverse vibration of the uniform cylinder.

V=0.2 m/s (*V*$_r$=5.17)
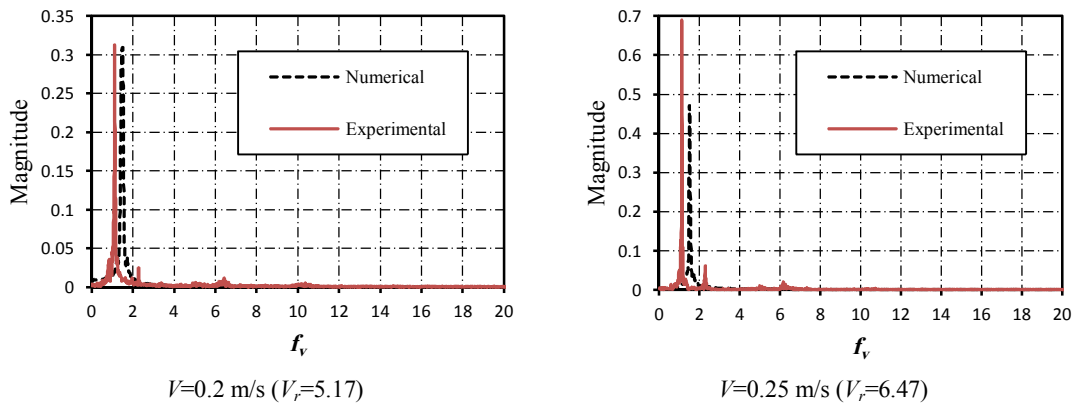

V=0.25 m/s (*V*$_r$=6.47)

Figure 8. Typical frequency contents of experimental and numerical transverse vibrations of the tapered cylinder.

Table 5. Lift and drag force coefficients on the elastically mounted tapered cylinder.

Circular cylinder	Reduced velocities	RMS lift coefficient	Mean drag coefficient
Tapered Cylinder	3.88	0.28	0.99
	5.18	0.24	1.18
	5.69	0.21	1.08
	6.47	0.23	1.07
	7.76	0.13	0.89
	10.35	0.16	0.88

The results presented in Figures 5 to 8 show that the numerical model can provide some acceptable predictions as compared to the in-water towing tank for the VIV of elastically mounted tapered and uniform circular cylinders. The numerical model, therefore may be used to further disclose essential characteristics of the VIV response of tapered circular cylinders.

3.2. Fixed against moving tapered cylinder

With an elastically mounted cylinder vibrating in the cross-flow direction, the wake flow field will be different from that of a stationary cylinder. Around the lock-in range, however, the vortices synchronize with the cylinder oscillations and the flow field becomes more two dimensional. Of interest is to use the numerical model to compare the flow fields at the wake of an elastically mounted and a fixed tapered cylinder around the lock-in range. The flow field conditions at a reduced velocity of 6.47 (V=0.25 m/s at Reynolds number of 7,000) is selected for this purpose. It is noted that the taper ratio remains the same and equals to 20 in the present experimental and numerical modellings.

Fourier analysis of the velocity fluctuations in the wake of the elastically mounted and fixed tapered cylinder at the reduced velocity of 6.47 are presented in Figure 9. The monitoring points have a coordinate of 3.14cm in stream-wise direction and 2.24cm in cross-stream direction from the cylinder axis. As it can be seen, for the case of the fixed tapered cylinder the dominant vortex shedding frequencies are constantly changing in different span-wise elevations. It changes from 1.7 to 2.6 Hz span-wise of the fixed cylinder. For the case of the elastically mounted tapered cylinder in the lock-in range the dominant vortex shedding frequencies, however, remain almost identical in the span-wise direction (around 1.5 Hz). Figure 9 also indicates that the flow field at the wake of the elastically mounted tapered cylinder becomes more two dimensional in the lock-in range. In other words the flow field in the wake of an elastically mounted cylinder (in the lock-in range) appears to much resemble that for a uniform cylinder while the flow field for the fixed cylinder considerably differs. The single frequency type of response was also observed for other test cases when the reduced transverse response grew above 0.3 (Figure 10). This seems to be in line with findings of other researchers in their experimental works. Techet et al. [19] studied the flow in the wake of forced vibrating tapered circular cylinders in towing tank experiments. The Reynolds numbers ranged from 400 to 1,500. They reported that within some parametric ranges no vortex cell was forming in the lock-in region and that a single frequency response dominated the entire span-wise length. They attributed this to the amplitude of vibration effects.

Time histories of the drag and lift force coefficient in the elastically mounted and fixed tapered circular cylinder at the reduced velocity of 6.47 are compared in Figure 11. As it can be seen the lift and drag force coefficient amplitudes of the elastically mounted cylinder are higher and more regulated compared to those for the fixed tapered cylinder. This seems to be an outcome of the synchronization of vortices with the elastically mounted cylinder at the lock-in range which increases the flow field two dimensionality. As mentioned before the increase of flow field two dimensionality will increase the vortices strength and consequently will increase the lift and drag coefficients [2].
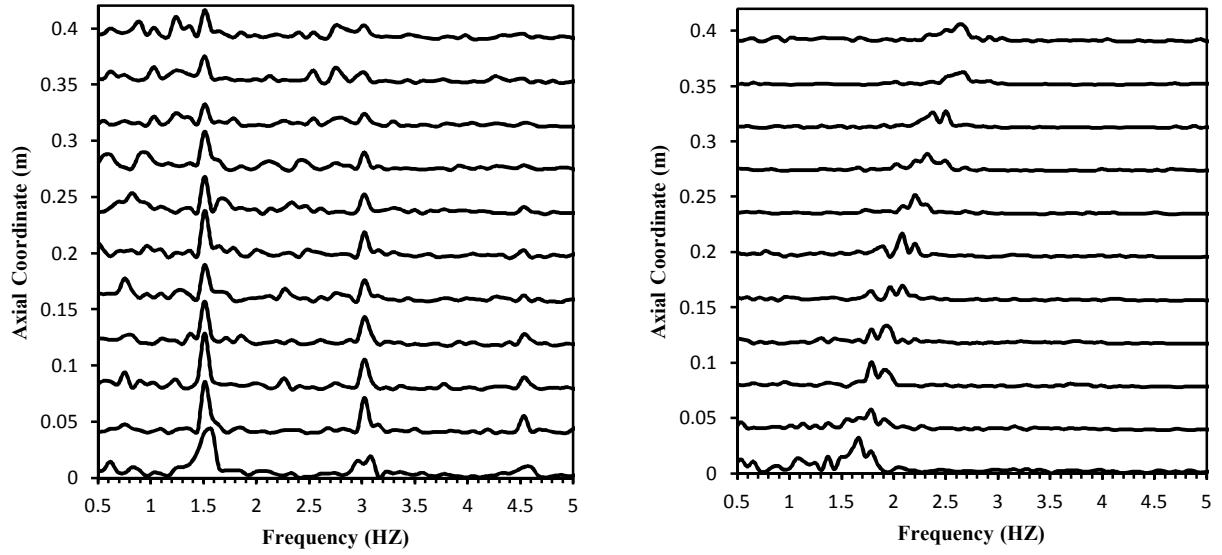
Figure 9. Fourier analysis of the velocity fluctuations at the reduced velocity of 6.47 in the wake of the elastically mounted (left) and fixed (right) tapered cylinder
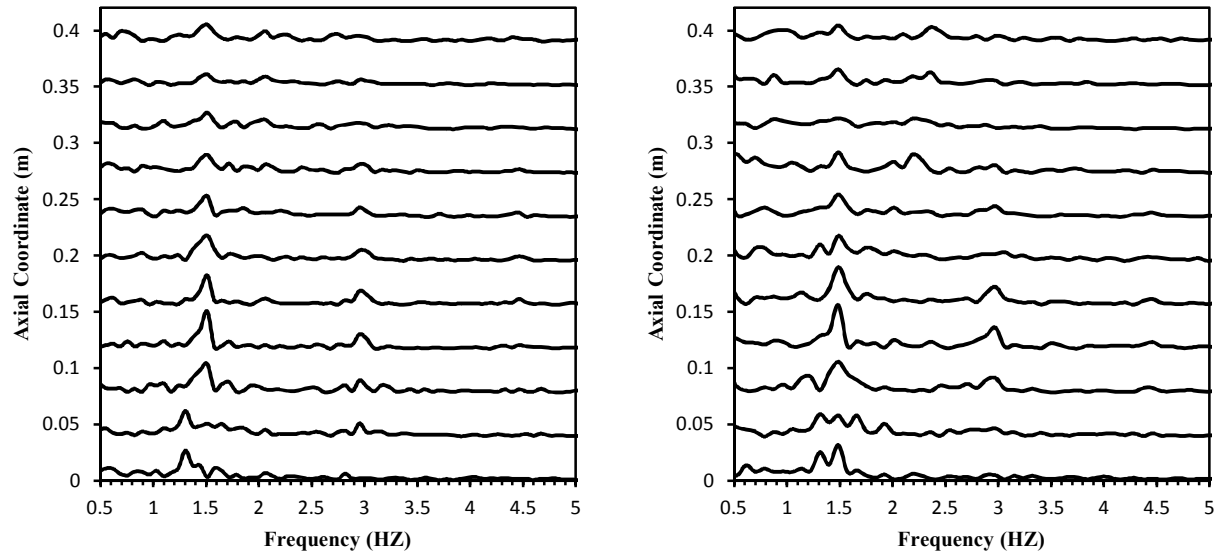

Figure 10. Fourier analysis of the velocity fluctuations at the reduced velocities of 5.17 (left) and 5.69 (right) in the wake of the elastically mounted tapered cylinder
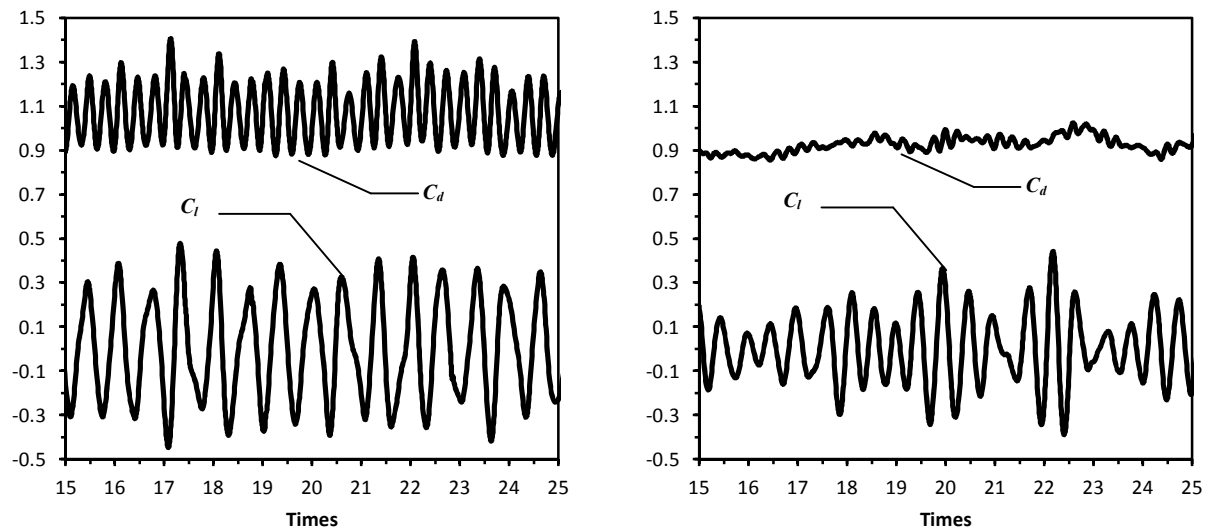

Figure 11. Drag (C_d) and lift (C_l) force coefficients time histories for the elastically mounted (left) and fixed (right) tapered circular cylinder at a reduced velocity of 6.47.

3.3. Cellular vortex shedding

Formation of span-wise cells within which shedding frequency is constant, or in other words cellular vortex shedding, is one of the key characteristics of the flow behind a stationary tapered cylinder [19]. In the current study and in order to specify the number of span-wise vortex cells, the Strouhal numbers along the cylinder axis are extracted from the numerical model and presented in Figure 12. The results are for a cylinder with a taper ratio of 20 in a Reynolds number of 7,000. The geometrical properties remain the same as those given in Table 2. A span-wise region with an unvarying Strouhal number represents a vortex cell. Each zone indicates a discrete shedding cell, with its own constant shedding frequency. From Figure 12, three to four distinctive shedding cells, along the fixed tapered cylinder axis, can be identified. This is while for the case of the elastically mounted tapered cylinder a single frequency almost dominates the whole span length of the cylinder. It means that with an elastically mounted tapered cylinder, in contrast to the stationary cylinder, around the lock-in range no cells are formed and that a unique frequency dominates the response of the cylinder over its entire span.
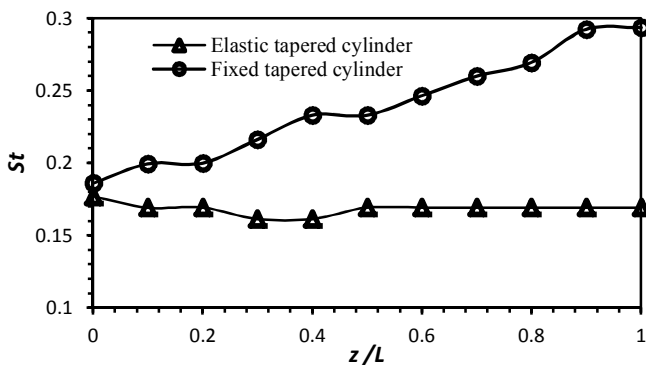

Figure 12. The Strouhal number (*St*) variation along the tapered cylinder axis (*z*) at a reduced velocity of 6.47.

3.4. Vortex splitting and oblique vortex shedding

By making use of pseudo-flow visualization techniques, which were developed by Wat [39], the possibility of vortex dislocations can be identified. Figure 13 gives sample numerical time histories of the velocity at arbitrary monitoring points in the wake of the stationary and elastically mounted tapered cylinder. The monitoring points have a coordinate of 3.14 cm in stream-wise direction and 2.24 cm in cross stream direction from the cylinder axis.

The red colours represent the peaks (local maxima) and the blue colours denote the valleys (local minima). The velocity peaks demonstrate the passageways of the vortices [17]. Therefore, continuous red areas in this figure represent the span-wise spreading of the vortex lines in the wake of the tapered cylinder. A kink in the vortex lines (see Figure 13), indicates the onset of a vortex splitting (or vortex dislocation). As shown in Figure 13, for the case of the elastically mounted tapered cylinder there are no obvious vortex dislocations along the span of the cylinder. Vortices are, however, apparently dislocated at the distance of 0.05 to 0.25 of the fixed tapered cylinder span.

3.5. Vorticity patterns

Inspection of the span-wise vorticity for the case of the elastically mounted tapered cylinder at a reduced velocity of 6.47 indicates that only 2S vortical patterns (two vortices per cycle) dominate the entire span of the cylinder. Figure 14-a illustrates the instantaneous isosurfaces of the total pressure at the Re=7,000 and reduced transverse amplitude of about 0.4. Straight distinct vortices along the span of the cylinder demonstrate formation of a uniform vortical pattern along the entire span of the cylinder without
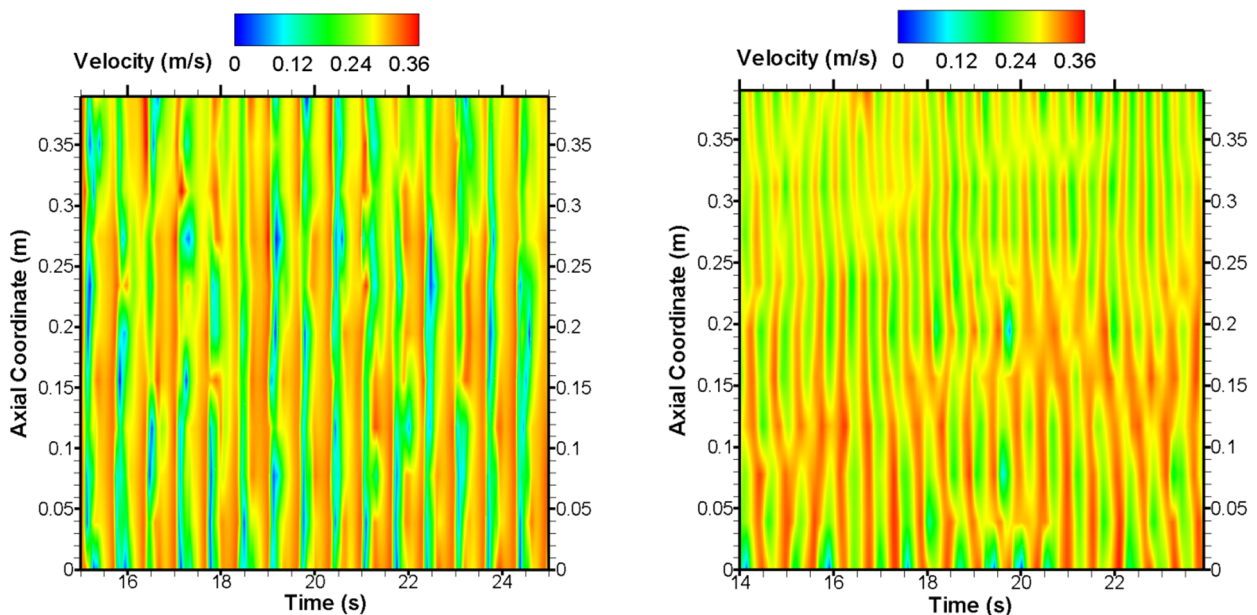

Figure 13. Pseudo-flow visualization. Contour lines of velocity (at a reduced velocity of 6.47) fluctuation at the wake of an elastically mounted (left) and fixed (right) tapered cylinder.

29

any vortex splitting. Strong obliquenesses in the vortex shedding behind the stationary tapered cylinder are clearly demonstrated in Figure 14-b. Figure 14-b also indicates the onset of vortex splitting in the wake of the fixed tapered cylinder.
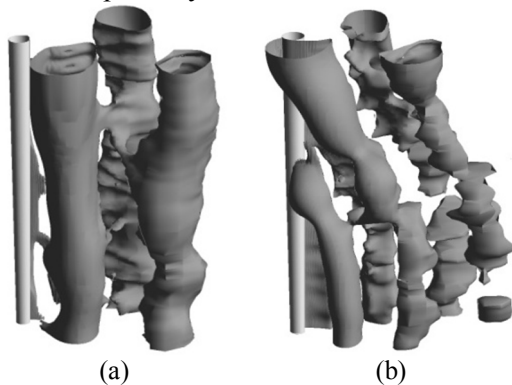

|(a)| |(b)|

Figure 14. (a). A 2S and vertically uniform vortical patterns along the span of the elastically mounted cylinder with no apparent vortex splitting (at V_r=6.47, Re=7,000 and reduced transverse amplitude of about 0.4). (b). Oblique vortex shedding with about three main vortex cells at the wake of the fixed tapered cylinder (at V_r=6.47).

4. Conclusions

In the present study, self excited transverse response of uniform and tapered circular cylinders are numerically simulated. The cylinders have medium mass ratios (5.93, 6.1) and low mass-damping parameters (0.0275, 0.0279). The model replicates an in-water towing tank experimental study conducted by the authors to investigate the VIV response of elastically mounted tapered cylinders. A fully coupled two way fluid structure interaction (FSI) analysis is used to simulate the phenomena of vortex induced vibration in vicinity of lock-in range. The transverse vibrations of uniform and tapered cylinders are compared against the experimental data. The numerical results reveal that the model is capable to reasonably well predict the initial and upper branches of the responses. It, however, falls short to properly predict the lower branch. Time histories of the transverse vibrations and lift and drag force coefficients of the elastically mounted uniform and tapered cylinders are also provided. The simulation results of the fixed and elastically mounted tapered cylinders are compared and discussed. The results indicate that the flow field in the case of the elastically mounted tapered cylinder is completely different from that for the fixed tapered cylinder. With the elastically mounted tapered cylinder no vortex cell appears to form in the lock-in region and a single frequency response dominates the entire length of the cylinder. A vertically uniform 2S vortical pattern along the span of the elastically mounted cylinder is observed through vortex visualization. This is for a reduced velocity of 6.47 in the lock-in range. However, the results of vortex visualization for the fixed tapered

cylinder reveal an oblique vortex shedding with about three main vortex cells along the cylinder span.

5. References

1- Zeinoddini, M., Tamimi, V. and Seif, M.S., (2013), *Stream-wise and cross-flow vortex induced vibrations of single tapered circular cylinders: An experimental study*, Journal of Applied Ocean Research, Vol. 42, p. 124-135.

2- Gabbai, R.D. and Benaroya, H., (2005), *An overview of modeling and experiments of vortex-induced vibration of circular cylinders*, Journal of Sound and Vibration, 282: 575.

3- Blackburn, H.M. and Karniadakis, G.E., (1993), *Two-and three-dimensional simulations of vortex-induced vibration of a circular cylinder*, In: Proceedings of the 3rd International Offshore and Polar Engineering Conference, Singapore, 3: 715–720

4- Newman, D.J. and Karniadakis, G.E., (1997), *A direct numerical simulation study of flow past a freely vibrating cable*, Journal of Fluids Mechanics, Vol. 344, p. 95-136.

5- Zhang, J. and Dalton, C., (1996), *Interaction of vortex-induced vibrations of a circular cylinder and a steady approach flow at a Reynolds number of 13,000*, Computers and Fluids, Vol. 25, p. 283–294.

6- Saltara, F., Meneghini, J.R. and Siquiera, C.L.R., (1998), *The simulation of vortex shedding from an oscillating circular cylinder*, In: Proceedings of the 8th International Offshore and Polar Engineering Conference, Montreal, Canada, 3:356-363.

7- Evangelinos, C., Lucor, D. and Karniadakis, G.E., (2000), *DNS-derived force distribution on flexible cylinders subject to vortex-induced vibration*, Journal of Fluids and Structures, Vol. 14, p. 429-440.

8- Tutar, M. and Holdo, A.E., (2000), *Large Eddy Simulation of a smooth circular cylinder oscillating normal to a uniform flow*, ASME Journal of Fluids Engineering, Vol. 122, p. 694-702.

9- Guilmineau, E. and Queutey, P., (2004), *Numerical simulation of vortex-induced vibration of a circular cylinder with low mass-damping in a turbulent flow*, Journal of Fluids and Structures, Vol. 19, p. 449-466.

10- Al-Jamal, H. and Dalton, C., (2004), *Vortex induced vibrations using Large Eddy Simulation at a moderate Reynolds number*, Journal of Fluids and Structures, Vol. 19, p. 73-92.

11- Saltara, F., D'Agostini Neto, A. and Lopez, J.I.H., (2011), *3D CFD simulation of vortex-induced vibration of cylinder*, International Journal of Offshore and Polar Engineering, Vol. 21, p. 192-197.

12- Jespersen, D.C. and Levit, C., (1990), *Numerical simulation of flow past a tapered cylinder*, NAS Technical Report RNR-90-021.

13- Vall`es, B., Andersson, H.I. and Jenssen, C.B., (2002), Oblique vortex shedding behind tapered

cylinders. Journal of Fluids and Structures, Vol. 16, p. 453-463.

14- Parnaudeau, P., Heitz, D., Lamballais, E., and Silvestrini, J.H., (2005), *Direct numerical simulations of vortex shedding behind cylinders with spanwise linear nonuniformity*, Proc. TSFP4, 111-116.

15- Narasimhamurthy, V.D., Schwertfirmk, F., Andersson, H.I. and Pettersen, B., (2006), *Simulation of unsteady flow past tapered circular cylinders using an Immersed Boundary Method*, In: European Conference on Computational Fluid Dynamics ECCOMAS CFD, Norwegian University of Science and Technology (NTNU), Dept. of Energy and Process.

16- Tamimi, V., Zeinoddini, M., Bakhtiari, A. and Golestani, M., (2012), *3D simulation of vortex shedding past tapered circular cylinders at subcritical Reynolds numbers*, In: The 31st International Conference on Ocean, Offshore and Arctic Engineering (OMAE 2012), 10-15 June, Rio de Janeiro, Brazil.

17- Hsiao, F.B. and Chiang, C.H., (1998), *Experimental study of cellular shedding vortices behind a tapered circular cylinder*, Experimental Thermal and Fluid Science, Vol. 17, p.179-188.

18- Hover, F.S., Techet, A.H. and Triantafyllou, M.S., (1998), *Forces on oscillating uniform and tapered cylinders in cross-flow*, Journal of Fluids Mechanics, Vol. 363, p. 97-114.

19- Techet, A.H., Hover, F.S. and Triantafyllou, M.S., (1998), *Vortical patterns behind a tapered cylinder oscillating transversely to a uniform flow*, Journal of Fluids Mechanics, Vol. 363, p. 79-96.

20- Löhner, R., Yang, C., Cebral, J., Baum, J.D., Luo, H., Pelessone, D. and Charman, C., (1995), *Fluid-structure interaction using a loose coupling algorithm and adaptive unstructured grids*, in Hafez, M., Oshima, K., editors, Computational Fluid Dynamics Review 1995, Wiley, Chichester.

21- Farhat, C., Lesoinne, M. and Maman, N., (1995), *Mixed explicit/implicit time integration of coupled aeroelastic problems: Three-field formulation, geometric conservation and distributed solution*, International Journal for Numerical Methods in Fluids, Vol. 21, p. 807-835.

22- Le Tallec, P. and Mouro, J., (2001), *Fluid structure interaction with large structural displacements*, Computer Methods in Applied Mechanics and Engineering, Vol. 190, p. 3039-3068.

23- Mok, D.P., (2001), *Partitionierte Lösungsansätze in der Strukturdynamik und der Fluid-Struktur-Interaktion*, Dissertation, Universität Stuttgart.

24- Hübner, B., Walhorn, E. and Dinkler, D., (2004), *A monolithic approach to fluid-structure interaction using space-time finite elements*, Computer Methods in Applied Mechanics and Engineering Vol. 193, p. 2087-2104.

25- Bathe, K.J. and Zhang, H., (2004), *Finite element developments for general fluid flows with structural interactions*, International Journal for Numerical Methods in Engineering, Vol. 60, p. 213-232.

26- Hron, J. and Turek, S., (2006), *A monolithic FEM solver for an ALE formulation of fluid-structure interaction with configuration for numerical benchmarking*, in Wesseling, P., On☐ate, E., Périaux, J., editors, Proceedings of the European Conference on Computational Fluid Dynamics, Delft.

27- Hübner, B. and Seidel, U., (2007), *Partitioned solution to strongly coupled hydroelastic systems arising in hydro turbine design*, 2nd IAHR International Meeting of the Workgroup on Cavitation and Dynamic Problems in Hydraulic Machinery and Systems Timisoara, Romania October 24 - 26, 2007.

28- ANSYS CFX Reference Guide. Release 12.0. ANSYS, Inc. Southpointe. 275 Technology Drive. ANSYS, Inc. April 2009.

29- Tamimi,V., Zeinoddini, M. and Bakhtiari, A., (2014), *Vortex Shedding Characteristics of Tapered Cylinders at Turbulent Wake*, Journal of Offshore Structure and Technology.

30- Tamimi, V., (2012), *Experimental and numerical study of VIV and WIV in single and tandem tapered circular cylinders*, Master's thesis, K.N.Toosi University of technology, Tehran, Iran, (In Persian).

31- Pope, S.B., (2000), *Turbulent flows*, Cambridge University Press.

32- Smagorinsky, J., (1963), *General circulation experiments with the primitive equations*, Month. Weath, Rev 93: 99-165.

33- Murakami, S., (1993), *Comparison of various turbulence models applied to a bluff body*, Journal of Wind Engineering and Industrial Aerodynamics, Vol. 46&47, p. 21-36.

34- Rodi, W., (1993), *On the simulation of turbulent flow past bluff bodies*, Journal of Wind Engineering and Industrial Aerodynamics, Vol. 46&47, p. 3-19.

35- Nicoud, F. and Ducros, F., (1999), *Subgrid-scale stress modelling based on the square of the velocity gradient tensor*, Flow, Turbulence and Combustion, Vol. 62, p. 183-200.

36- Germano, M., Piomelli, U., Moin, P. and Cabot, W.H., (1991), *A dynamic subgrid-scale eddy viscosity model*, Phys. Fluids, A 3 (7), p. 1760-1765.

37- Lilly, D.K., (1992), *A proposed modification of the Germano subgrid-scale closure method*, Phys. Fluids, A 4 (3), p. 633-635.

38- Dong, S. and Karniadakis, G.E., (2005), *DNS of flow past a stationary and oscillating cylinder at Re 10000*, Journal of Fluids and Structures, Vol. 20, p. 519–531.

39- Wat, J.K., (1988), *The unsteady and radiation behaviour of a jet*, Ph.D. Thesis, Department of Aerospace Engineering, University of Southern California, Los Angeles, CA.